Original containing color plates: All DTIC reproductions will be in black and white"

DTIC ELECTE APR 29 1993 S C D

(2)

ARMY RESEARCH LABORATORY

ARL

AD-A263 299

A Computational Study of The Base Region Flow Field For The M865 Projectile

Jubaraj Sahu

ARL-TR-109 April 1993

APPROVED FOR PUBLIC RELEASE; DISTRIBUTION IS UNLIMITED.

93-09034

93 4 23 011

REPORT DOCUMENTATION PAGE

Form Approved
OMB No. 0704-0188

Public reporting burden for this collection of information is estimated to average 1 hour per response, including the time for reviewing instructions, searching existing data sources, gathering and maintaining the data needed, and completing and reviewing the collection of information. Send comments regarding this burden estimate or any other aspect of this collection of information, including suggestions for reducing this burden, to Washington Headquarters Services, Directorate for Information Operations and Reports, 1215 Jefferson Davis Highway, Suite 1204, Arlington, VA 22202-4302, and to the Office of Management and Budget, Paperwork Reduction Project (0704-0188), Washington, DC 20503.

1. AGENCY USE ONLY (Leave blank)	2. REPORT DATE	3. REPORT TYPE AND DATES COVERED
	April 1993	Final, November 1990 - June 1991

4. TITLE AND SUBTITLE

A COMPUTATIONAL STUDY OF THE BASE REGION FLOW FIELD FOR THE M865 PROJECTILE

5. FUNDING NUMBERS

PR: 1L161102AH43
WO: 61102A-00-001 AJ

6. AUTHOR(S)

JUBARAJ SAHU

7. PERFORMING ORGANIZATION NAME(S) AND ADDRESS(ES)

U.S. Army Research Laboratory
ATTN: AMSRL-WT-PB
Aberdeen Proving Ground, MD 21005-5066

8. PERFORMING ORGANIZATION REPORT NUMBER

9. SPONSORING / MONITORING AGENCY NAME(S) AND ADDRESS(ES)

US Army Research Laboratory
ATTN: AMSRL-OP-CI-B (Tech Lib)
Aberdeen Proving Ground, Maryland 21005-5066

10. SPONSORING / MONITORING AGENCY REPORT NUMBER

ARL-TR-109

11. SUPPLEMENTARY NOTES

The author wishes to thank the Armament Research, Development and Engineering Center (ARDEC), Picatinny Arsenal, New Jersey, for the financial support of this work.

This report supersedes BRL-IMR-955, January 1991.

12a. DISTRIBUTION / AVAILABILITY STATEMENT

Approved for public release; distribution is unlimited.

12b. DISTRIBUTION CODE

13. ABSTRACT (Maximum 200 words)

Recent firing tests for the M865 projectile have indicated that for reasons unknown, the tracer in the base cavity region does not remain visible during the entire flight. To assist in analyzing this problem, a computational study has begun to examine the base region flow field for this projectile including the base cavity. Flow computations for this projectile have been performed at various supersonic Mach numbers, $2 < M < 5$ and alpha = 0.0 degree using a time marching Navier-Stokes code. The computed results show sharp changes in the centerline pressure distributions in the base region near $M = 3$. This unexpected behavior may not be desirable and could be part of the problem. To minimize these pressure oscillations, several proposed configuration changes have been made in the afterbody base cavity region and computations have been performed for these modified configurations to analyze the effects on the flow field. One of these configurations with a new base cavity shape was found to improve the base region flow field. A modified version of this new base cavity has been flight tested and the results revealed some improvement in the visibility of the tracer compared to the original configuration.

14. SUBJECT TERMS	15. NUMBER OF PAGES
Aerodynamics; axisymmetric flow; base flow; wake; cavity.	33
	16. PRICE CODE

17. SECURITY CLASSIFICATION OF REPORT	18. SECURITY CLASSIFICATION OF THIS PAGE	19. SECURITY CLASSIFICATION OF ABSTRACT	20. LIMITATION OF ABSTRACT
UNCLASSIFIED	UNCLASSIFIED	UNCLASSIFIED	UL

INTENTIONALLY LEFT BLANK.

TABLE OF CONTENTS

INTENTIONALLY LEFT BLANK.

LIST OF FIGURES

1. INTRODUCTION

The ability to compute the base region flow field for projectile configurations using Navier-Stokes computational techniques has been developed over the past few years (Sahu, Nietubicz, and Steger 1983; Sahu 1987a, 1987b; Sahu, Nietubicz, and Heavey 1988). This capability is very important for determining aerodynamic coefficient data including the total aerodynamic drag. Base flow calculations to date have included both the solid base as well as base cavity configurations. The M865 projectile has a base cavity which contains a tracer. Ideally, the tracer should be visible for the entire flight of the projectile. Recent firing tests for this projectile have indicated that after about 2 kilometers (Mach number approximately 3) the tracer is no longer visible. The reasons for this behavior are not known at this time. A computational study for this projectile was thus undertaken with emphasis on the base region flow field. The aim is to find out if any flow irregularities occur in the base region and to correct for such behavior by making simple configuration changes in the afterbody/base cavity shape.

Flow field computations for the M865 projectile have been performed at various supersonic Mach numbers, $2 < M < 5$ and $\alpha = 0.0^0$ using a recently developed three plane version of a three dimensional (3D) Navier-Stokes code. The solution technique, numerical algorithm and composite grid scheme are described in the next section. The composite grid or zonal scheme allows better geometric modeling of the base region and preserves the actual base corner. Computations have also been performed for several modified afterbody/base cavity configurations to examine the effects of these changes on the flow fields much like a numerical wind tunnel. The computed results show both the qualitative and quantitative features of the base region flow field.

2. SOLUTION TECHNIQUE

The complete set of time-dependent thin-layer Navier-Stokes equations is solved numerically to obtain a solution to this problem. The numerical technique used is an implicit finite difference scheme. Although time-dependent calculations are made, the transient flow is not of primary interest at the present time. The steady flow, which is the desired result, is obtained in a time asymptotic fashion.

2.1 Governing Equations. The complete set of three dimensional, time dependent, generalized geometry, thin-layer, Navier-Stokes equations for general spatial coordinates

ξ, η, ζ can be written as (Pulliam and Steger 1982):

$$\partial_\tau \hat{q} + \partial_\xi \hat{F} + \partial_\eta \hat{G} + \partial_\zeta \hat{H} = Re^{-1} \partial_\zeta \hat{S} \tag{1}$$

where

$$\begin{aligned} \xi &= \xi(x,y,z,t) && \text{- longitudinal coordinate} \\ \eta &= \eta(x,y,z,t) && \text{- circumferential coordinate} \\ \zeta &= \zeta(x,y,z,t) && \text{- nearly normal coordinate} \\ \tau &= t && \text{- time} \end{aligned}$$

The vector $\hat{q}$ contains the dependent variables [ρ,ρu, ρv,ρw,e] and the flux vectors $\hat{F}$,$\hat{G}$,$\hat{H}$ contain terms which arise from the conservation of mass, momentum and energy. In equation (1), the thin-layer approximation is used and the viscous terms involving velocity gradients in both the longitudinal and circumferential directions are neglected. The viscous terms are retained, however, for velocity gradients in a direction nearly normal to the surface where large flow gradients exist. These viscous terms in ζ are collected into the vector $\hat{S}$. Although not shown in equation (1), similar thin-layer viscous terms are also added in the longitudinal direction in the base region. Details of the governing equations can be found in Pulliam and Steger (1982).

2.2 Numerical Technique. The numerical algorithm used is an implicit approximately factored scheme with central differencing in the η and ζ directions and upwinding in the ξ direction. The smoothing terms used in the present study in the η and ζ directions are a blend of second order and fourth order terms. The idea here is to use second order difference near shocks. For the computation of turbulent flows, a two-layer Baldwin-Lomax (1978) algebraic turbulence model is used.

For simplicity, all the boundary conditions have been imposed explicitly. On the body surface, the no-slip boundary condition is used and the wall temperature is specified. Free stream boundary conditions are used at the inflow boundary. A non-reflection boundary condition procedure is used at the outer boundary. A symmetry boundary condition is imposed at the circumferential edges of the grid while a simple extrapolation is used at the downstream boundary. A combination of symmetry and extrapolation boundary condition is used at the center line (axis). The flow is initially set to free stream conditions everywhere and then advanced in time until a steady state solution is obtained. Further details of the numerical algorithm and boundary conditions can be found in Sahu and Steger (1988).

2.3 Composite Grid Scheme. In the present work, a simple composite grid scheme (Sahu and Steger 1987) has been used. Here, a large single grid is split into a number of

smaller grids so that computations can be performed on each of these grids separately. These grids use the available core memory one grid at a time, while the remaining grids are stored on an external disk storage device such as the solid state disk device (SSD) of the Cray X-MP/48 computer. The use of a composite grid scheme requires special care in storing and fetching the interface boundary data , i.e., the communication between the various zones. In the present scheme, there is a one to one mapping of the grid points at the interface boundaries. Thus, no interpolations are required. Details of the data storage, data transfer and other pertinent information such as metric and differencing accuracy at the interfaces can be found in the work of Sahu and Steger (1988) and Sahu (1988). This scheme has been successfully used by Sahu (1988) to compute three dimensional transonic flow over two projectiles and the same technique was also applied to a more complicated projectile with base cavities (Sahu and Nietubicz 1989). The present work is a further application of this technique to the M865 projectile with the base cavity where the zonal topology is very desirable.

3. RESULTS

Numerical computations have been made for the M865 projectile with the original and modified base cavities. Computations have been made at various supersonic speeds $2 < M_\infty < 5$ and $\alpha = 0.0^0$. Atmospheric flight conditions were used.

The M865 projectile is a 12.32 caliber cone-cylinder-flare projectile. It consists of a 3.43 caliber conical nose, a 6.72 caliber cylindrical section, and a 2.13 caliber 14^0 flare. The area of interest is the flow field in the near wake or the base region. Figure 1 shows the computational grid around the projectile. It consists of four zones: a small zone near the nose of the projectile, one over the rest of the body up the base corner, one in the base region or the wake, and the last one inside the base cavity region. The number of grid points used in these four zones are 20x60, 261x60, 84x119, and 54x30, respectively. The grid points are clustered near the body surface to capture the viscous turbulent boundary layer. As seen in this figure, the outer boundary is placed very close to the body since the flow of interest is supersonic and a non-reflection boundary condition is used at this boundary. An expanded view of the base region grid is shown in Figure 2 for the original afterbody. This figure shows the grid point clustering near the base corner and in the free shear layer region. This is done in an attempt to put more grid points in the regions where flow field gradients are large. Other afterbody/base cavity shapes have been considered. For each of these shapes, a new grid has been obtained. For most of the afterbody configurations the grids in the base cavity and the wake are changed.

A few qualitative results are presented next. Figure 3 shows the pressure contours for the M865 projectile for various supersonic Mach numbers, M = 2, 3, 4, and 5. As expected, it shows the shock wave emanating from the nose of the projectile. A strong shock wave is also seen to originate from the cylinder-flare junction. This is followed by the flow expansion at the base corner. As shown in the figure, the outer boundary is placed close to the projectile and a non-reflection boundary condition procedure is used. The shock waves and the expansion waves pass through this boundary rather smoothly. As Mach number is increased, the shocks get stronger and the shock angle decreases. Figure 4 shows the centerline pressure distribution as a function of the longitudinal position, X/D. Here, X/D is measured from the base so that the base cavity region corresponds to negative X/D. In the base cavity region, the centerline pressure increases as the base cavity wall is approached. In addition, the pressure level in this region decreases with an increase in Mach number. It is also interesting to note the unexpected pressure oscillations or irregularities near X/D = 0 for all Mach numbers except M = 5.0 . The pressure peak or oscillation is the largest at M =3. This is undesirable and could possibly affect the performance of the tracer. Figure 5 shows the pressure contours in the base region at M = 3. Again this figure clearly shows that sharp changes in pressure shown as a dark band occur on the centerline near X/D = 0. This behavior in the pressure distribution is not desirable and should be eliminated or at least reduced. For this purpose, several numerical configuration changes have been made in the afterbody/base cavity region. Computations have been performed for the modified afterbody/base cavity configurations and an analysis of the effect of these changes on the flow field was performed.

The first configuration change was to reduce the base cavity angle by half. This changes the base cavity shape while the outer flare remains unchanged. Computed results have been obtained for this configuration at $2 < M < 3.5$. The wake centerline pressure distribution for this case at M = 3.0 is shown in Figure 6 and compared with that of the original configuration. As seen in this figure, the modified configuration clearly produces a smoother pressure distribution than the original configuration. Figure 7 shows the pressure contours in the base region for the new configuration. Again, this plot shows much smoother behavior in the pressure contours than the original base cavity. Figure 8 shows the wake centerline pressure distributions for all Mach numbers computed for both the original and modified base cavities. For the original configuration, large pressure oscillations are seen at all Mach numbers except at M = 3.5 near X/D = 0. For the modified configuration or base cavity shape, these oscillations are reduced considerably and the distributions are smoother at all speeds examined.

The second modified configuration keeps the original base cavity shape unchanged. How-

ever, the afterbody flare is clipped near the base corner resulting in a cylindrical portion. Figure 9 shows the pressure contours in the base region for this configuration. This plot shows a similar behavior in the pressure contours to that observed for the original configuration. The dark region indicates a sharp pressure change and occurs a little more inside the cavity than the original configuration. This shift in the location of the oscillations can be seen more clearly in the centerline pressure distribution shown in Figure 10 compared with the original results. The magnitude of the oscillations is similar for both cases.

The third configuration is similar to the first one in that the outer flare remains unchanged and only the base cavity shape is changed. The base cavity for this design comes from a combination of base cavity shapes with the original configuration and configuration 1. Figure 11 shows the pressure contours in the base region for this configuration. Again, this plot shows smoother behavior in the pressure distribution than the original base cavity, although not as smooth as the first modified configuration. The wake centerline pressure distribution for this case is shown in Figure 12. As seen in this figure, the pressure oscillation near X/D = 0 is smoothed out; however, another pressure irregularity shows up near X/D = -0.5.

The wake centerline pressure distributions for the original configuration as well as the modified configurations are shown in Figure 13. As stated before, the pressure oscillations are found to be large for the original configuration and configuration 2. A change made to the afterbody flare (configuration 2) just shifts the location of these oscillations. In both of these cases, no change was made in the base cavity shape. It is also clear from this figure that any change made to the base cavity shape has a much larger effect on the base region flow field than the change in the shape of the outer flare. The two cases (configurations 1 and 3) where the base cavity shape was changed show smoother behavior compared to the others. Among these two configurations, configuration 1 has the most smooth behavior.

The results described above were sent to the Armament Research Development and Engineering Center (ARDEC) at Dover, New Jersey to assist them with the development of the M865 projectile. Based on the present computational results and other considerations, a new afterbody configuration was suggested with a change only in the base cavity region. The base cavity angle was chosen to be close to that of the modified configuration 1 which, as described above, gave the best computational result. However, the depth of the base cavity was reduced considerably from that of the modified configuration 1. Firing tests were then conducted for the modified M865 projectile with the new cavity. The results revealed some improvements in the visibility of the tracer when compared to the original configuration. Computations have been made for this new configuration and the results are shown in Figures 14 and 15. Figure 14 shows the pressure contours in the base region for this configuration. It shows smoother behavior in the pressure distribution than the original

base cavity but, not as smooth as was predicted with the modified configuration 1. The wake centerline pressure distribution is shown in Figure 15. As seen in this figure, pressure oscillations still exist near X/D = 0 for the ARDEC modified configuration and the pressure distribution is not as smooth as that found with the modified configuration 1.

The next three figures (Figures 16, 17 and 18) show the velocity vectors in the base region for the original shape, modified configuration 1 and the ARDEC modified configuration, respectively. The recirculatory flow in the near wake region and the base cavity is clearly evident. The primary recirculation zone extends into the base cavity region for all configurations. This zone is is more well defined for the modified configuration 1 (Figure 17) and the ARDEC modified configuration (Figure 18) than the original configuration (Figure 16). As expected, the secondary separation region near the base corner is affected by the base height for all configurations. The secondary separation zone for the modified configuration 1 is bigger than that obtained with the original configuration. This change in the secondary separation flow and the base height affects the base drag. The base drag for all configurations including the original one is shown in Figure 19. Flow field computations have also been made for a configuration with a flat base (without any base cavity) for comparison purpose.

The base drag for this case is included in Figure 19. As seen in this figure, the base drag for the solid base is the largest and is reduced by the changes made in the afterbody configurations. The base drag for the case where the outer flare was clipped is the lowest and is less than half that of the flat base case. For the other configurations the outer flare remained unchanged and different base cavity shapes have been used. The base drag is reduced by $4\% to 30\%$ due to the various base cavities. The original base cavity configuration (second from the right) has the lowest base drag among the configurations where only base cavity was changed. The modified configuration 1 which showed the smoothest behavior in the base region flow field and the ARDEC configuration have slightly higher base drag than the original configuration. Also shown here is the result of another configuration with a rectangular base cavity. The base drag for this configuration is slightly less than that of the flat base case. A careful look at these results reveal larger reduction in base drag with larger reduction in the base height (or base area). It can also be noted that the effect due to change in the depth of the base cavity is rather small as can be seen with configurations 3,4, and 5. Although not shown here, the largest base drag reduction due to the base cavity alone compared to the flat base case corresponds to about 12% reduction in the total drag.

Figure 20 shows the pressure contours for the M865 projectile with the original base cavity at M = 3. It shows the very high pressure regions which occur near the nose and the flare sections of the projectile and the low pressure region in the near wake. It shows the shock wave emanating from the nose of the projectile. A strong shock wave originates

from the cylinder-flare junction. This is followed by the flow expansion at the base corner which is followed by a recompression shock downstream of the base. Figure 21 shows the comparison of the pressure contours in the base region for the original configuration, modified configuration 1, and the ARDEC modified configuration. The flow expansion at the base corner and the recompression downstream of the base are clearly in this figure. The very low pressure region is shown in blue. As seen in this figure, the original base configuration contains a large region of pressure oscillations or irregularities. The modified configuration 1 shows a much smoother near wake flow field. The pressure irregularities have been reduced considerably. The ARDEC modified configuration shows a smaller reduction in the pressure irregularities compared to that of the modified configuration 1.

4. CONCLUDING REMARKS

A computational study has been made to examine the base region flow field for the M865 projectile which contains a base cavity. Flow computations for this projectile have been performed at various supersonic Mach numbers, $2 < M < 5$ and $\alpha = 0.0^0$ using a recently developed three plane version of a 3D Navier-Stokes code.

The computed results show the qualitative features of the base region flow field for the M865 projectile. The computed centerline pressure in the near wake shows smooth behavior for M = 5. However, as Mach number decreases, sharp changes in this pressure distribution can be seen to develop, especially at M = 3 and 2.5. To eliminate, or at least reduce, these oscillations in the pressure distribution, several proposed configuration changes have been made in the afterbody/base cavity region. Computations have been performed for these modified afterbody/base cavity configurations to analyze the effect of these changes on the flow fields. Of these configurations, the modified configuration 1 with a new base cavity shape improves the base region flow field. The computed results obtained with this configuration show the most improvement in the base region flow field including the wake centerline pressure distribution at M = 3 and 2.5.

Based on these computational results and other considerations, a new afterbody configuration was chosen for testing by ARDEC. The firing tests conducted for the M865 projectile with this ARDEC modified base cavity configuration revealed some improvements in the visibility of the tracer compared to the original configuration. Computations have been made for this configuration and the results still indicate the presence of pressure oscillations or irregularities in the base region. As a by-product of the computational analysis, the base drag for these afterbody configurations were examined. The base drag is reduced by $4-30\%$ due to these base cavities compared to a solid flat base.

The results presented in this report do not include the effect of the tracer material. This effect is expected to be small. However, the same computational technique can be used to include this effect by using mass injection in the base region, if desired.

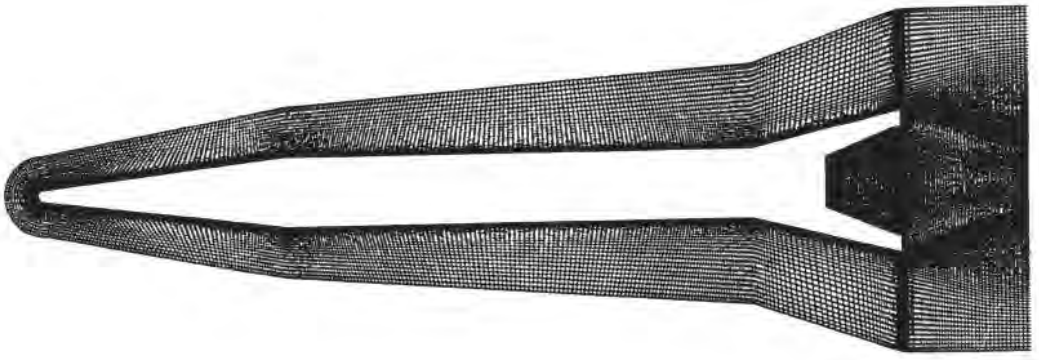

Figure 1. Computational grid for the projectile.

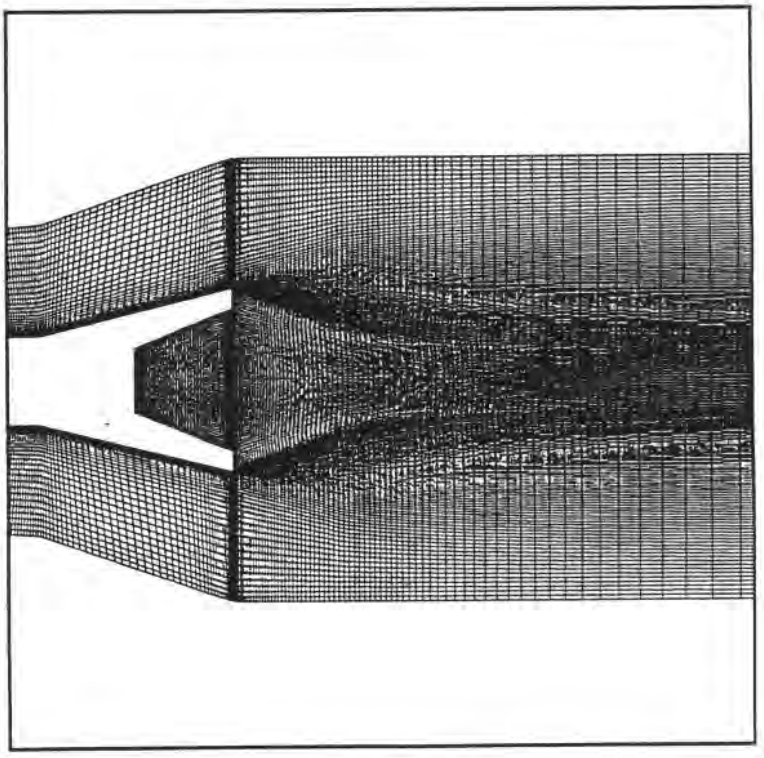

Figure 2. Expanded view of the base region grid.

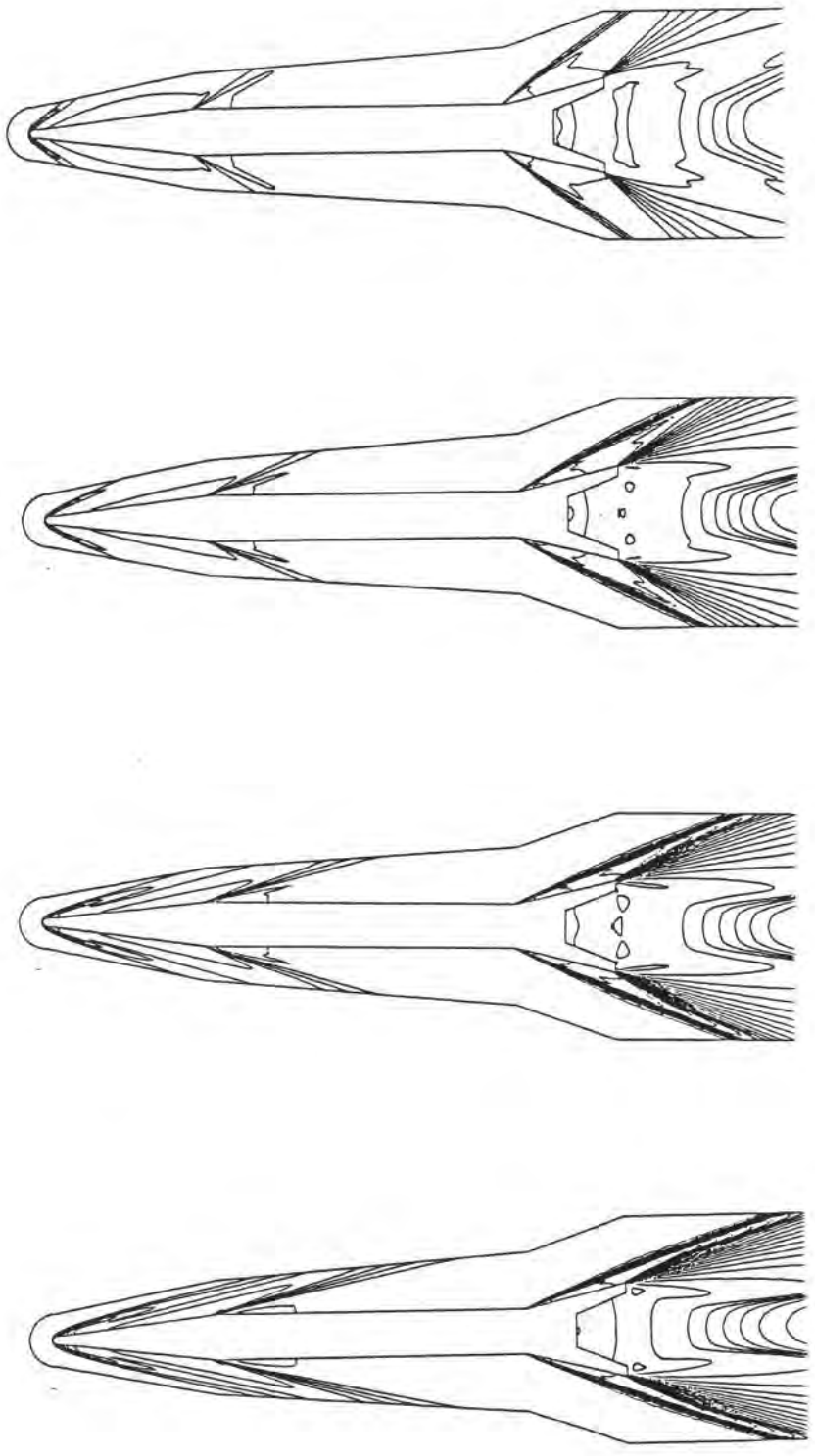

Figure 3. Pressure contours for the projectile, $\alpha = 0.0^0$, M_∞= 2,3,4,5 from top to bottom, (Original configuration).

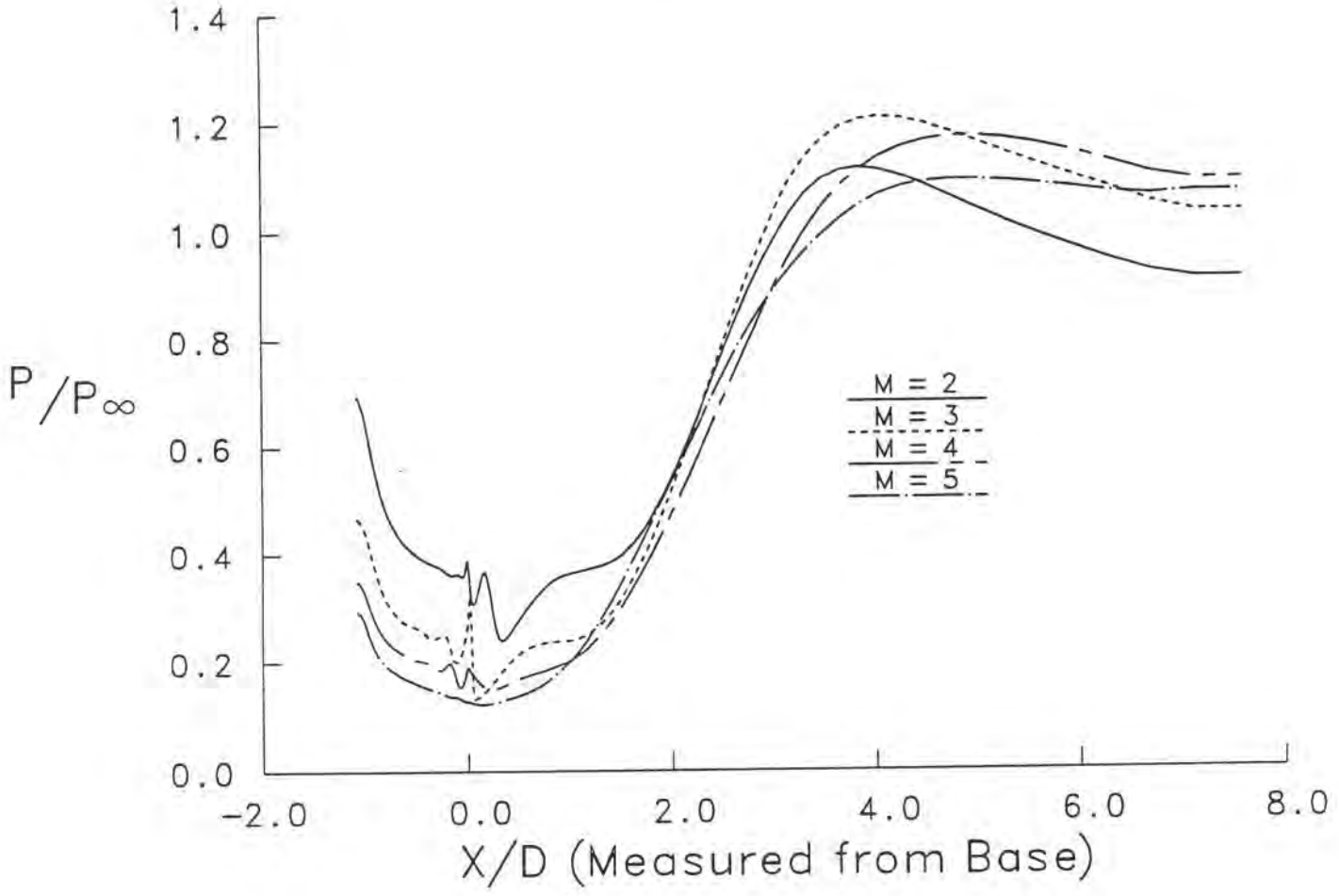

Figure 4. Wake Centerline Pressure distributions, $\alpha = 0.0^0$, (Original configuration).

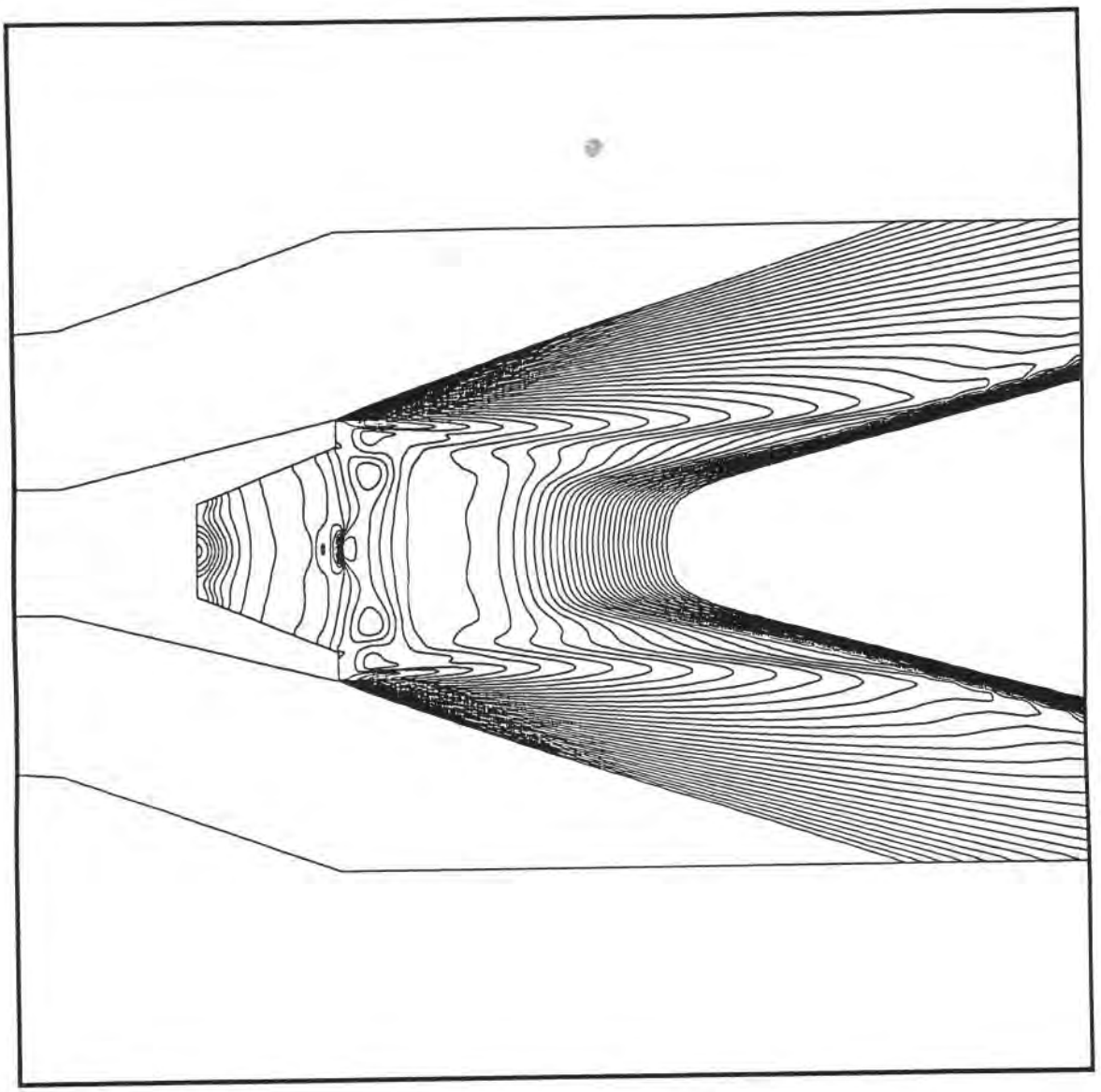

Figure 5. Pressure contours in the base region, M_∞=3.0, $\alpha = 0.0^0$, (Original configuration).

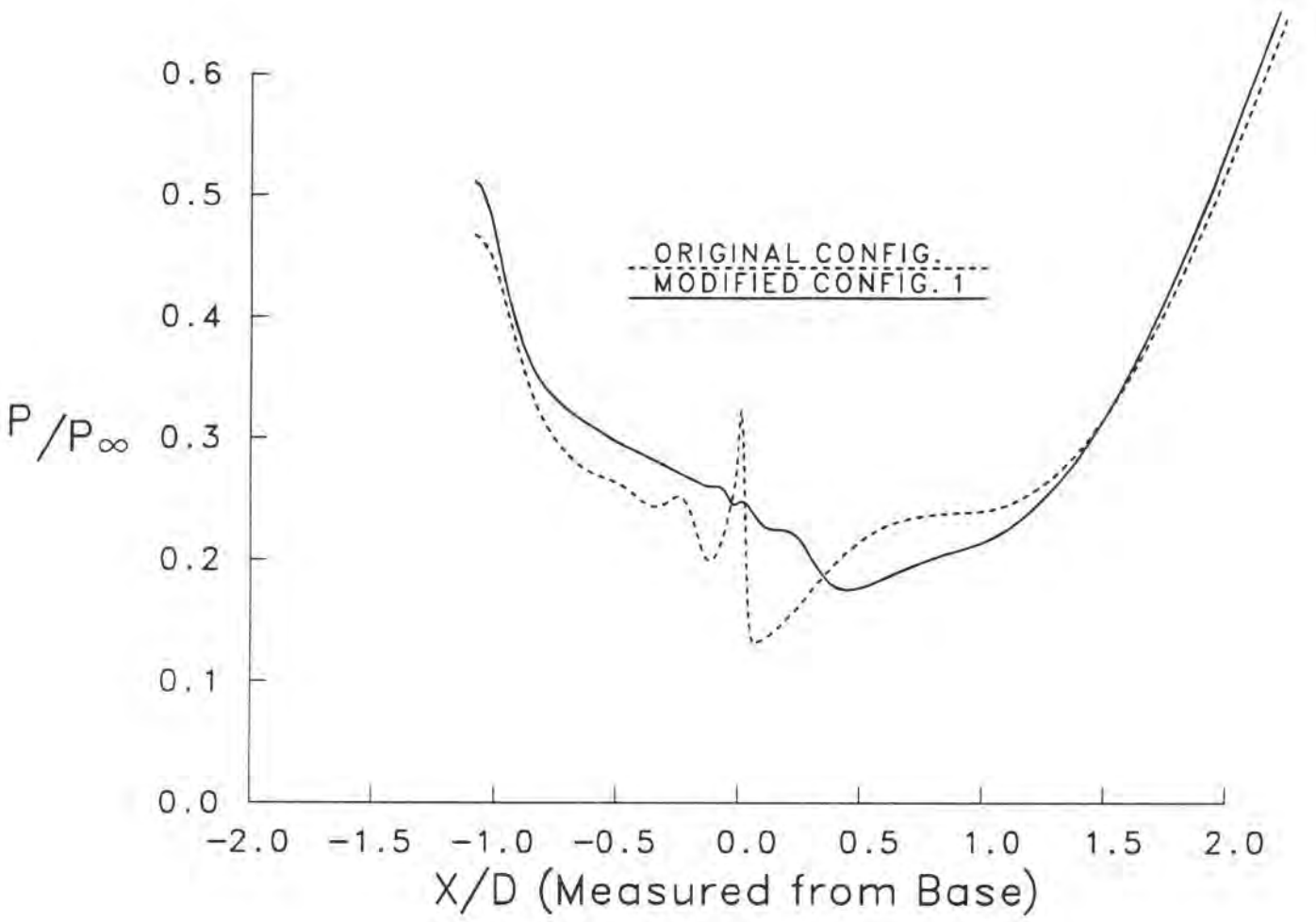

Figure 6. Wake Centerline Pressure distributions, M_∞=3.0, $\alpha = 0.0^0$, (Modified configuration 1).

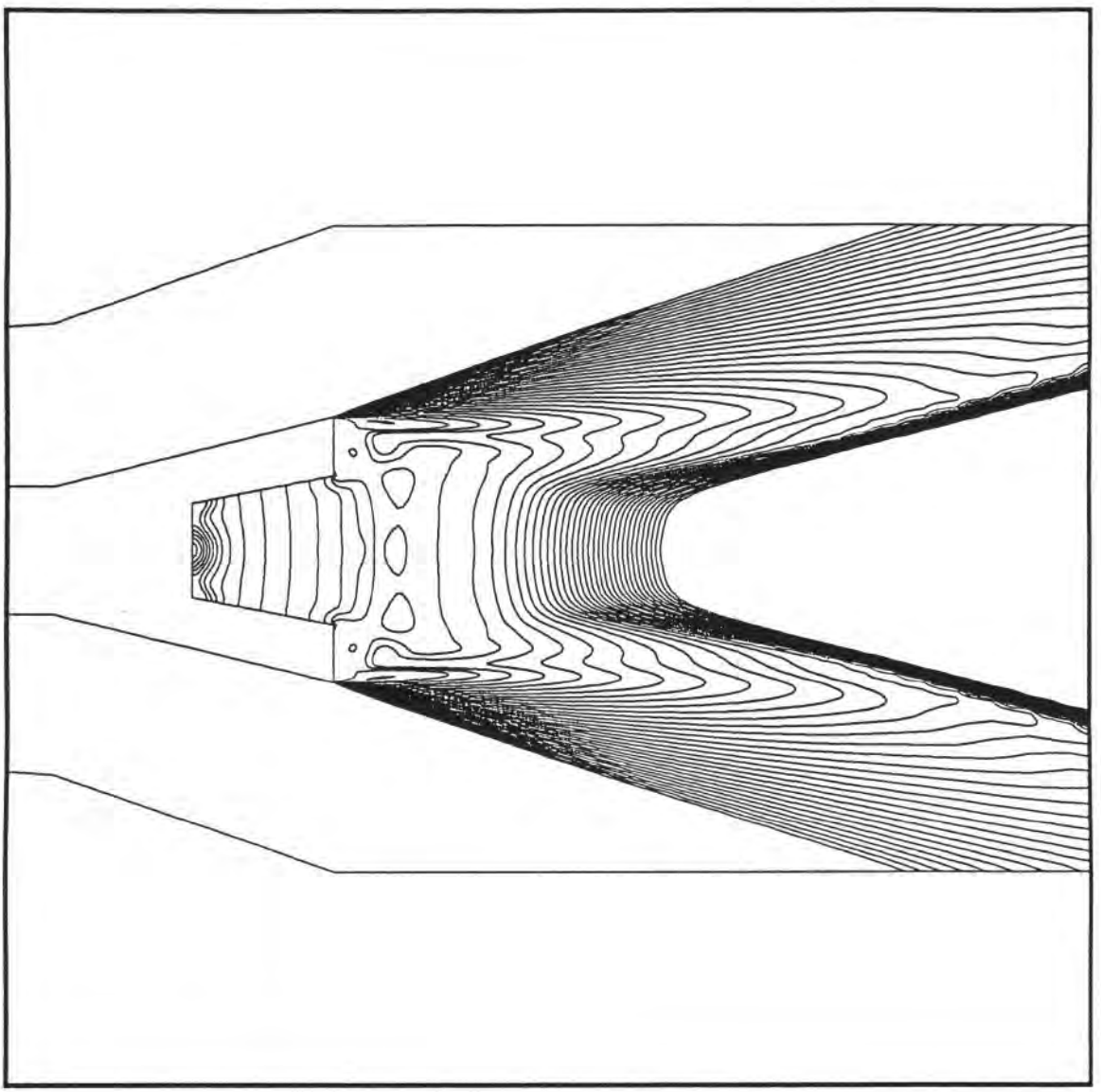

Figure 7. Pressure contours in the base region, M_∞=3.0, $\alpha = 0.0^0$, (Modified configuration 1).

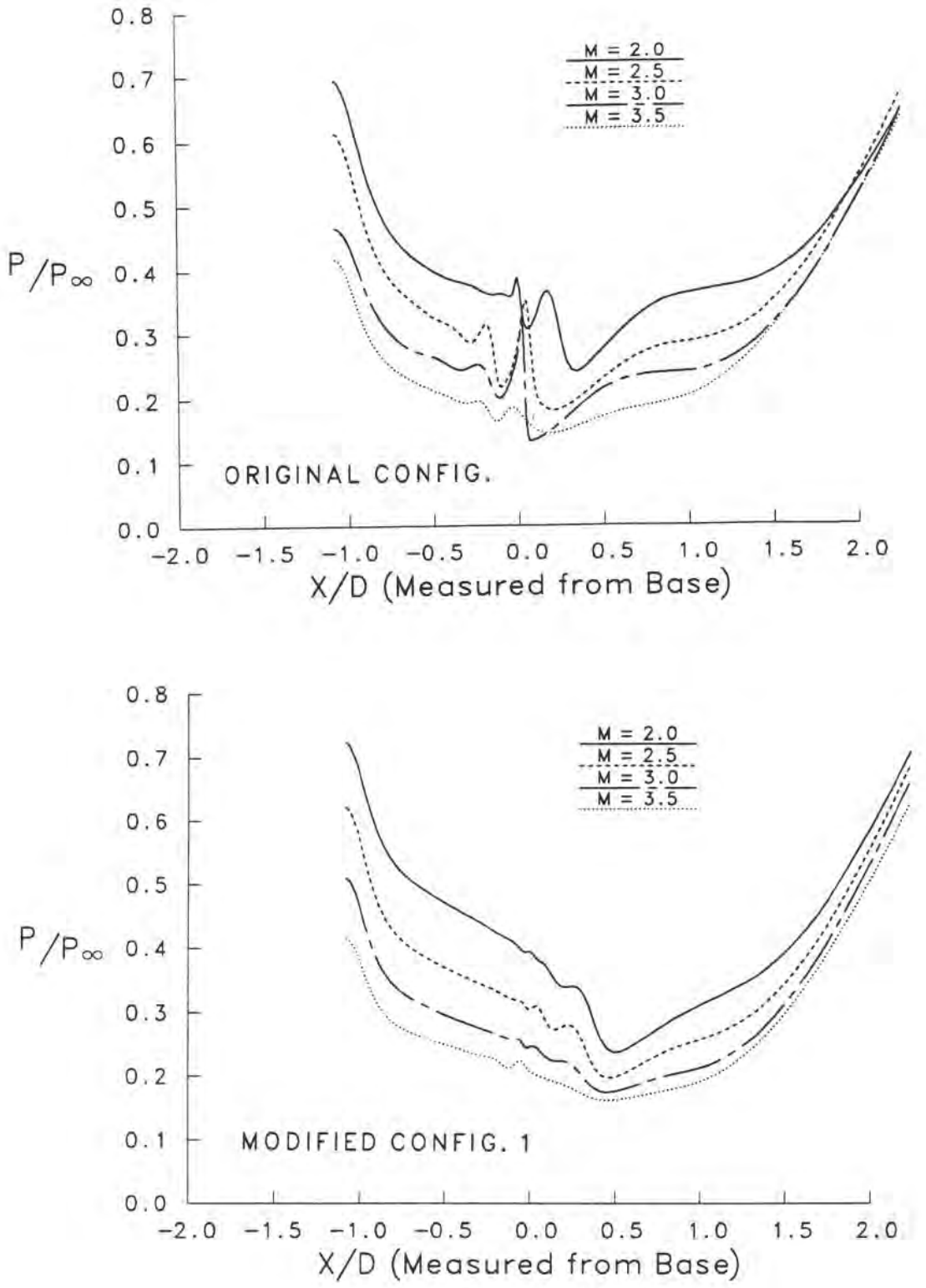

Figure 8. Wake Centerline Pressure distributions, $\alpha = 0.0^0$, (Original configuration and Modified configuration 1).

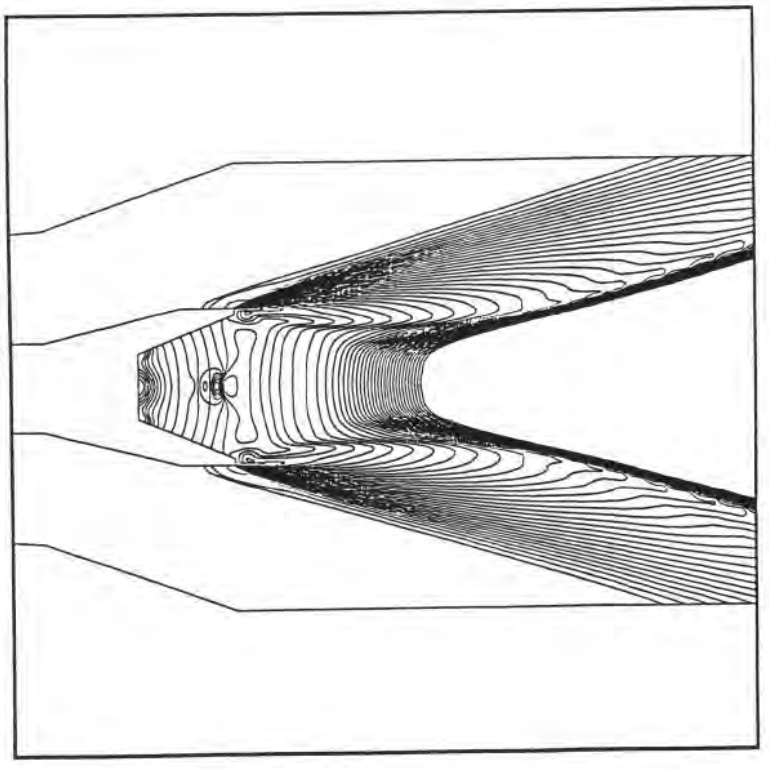

Figure 9. Pressure contours in the base region, M_∞=3.0, $\alpha = 0.0^0$, (Modified configuration 2).

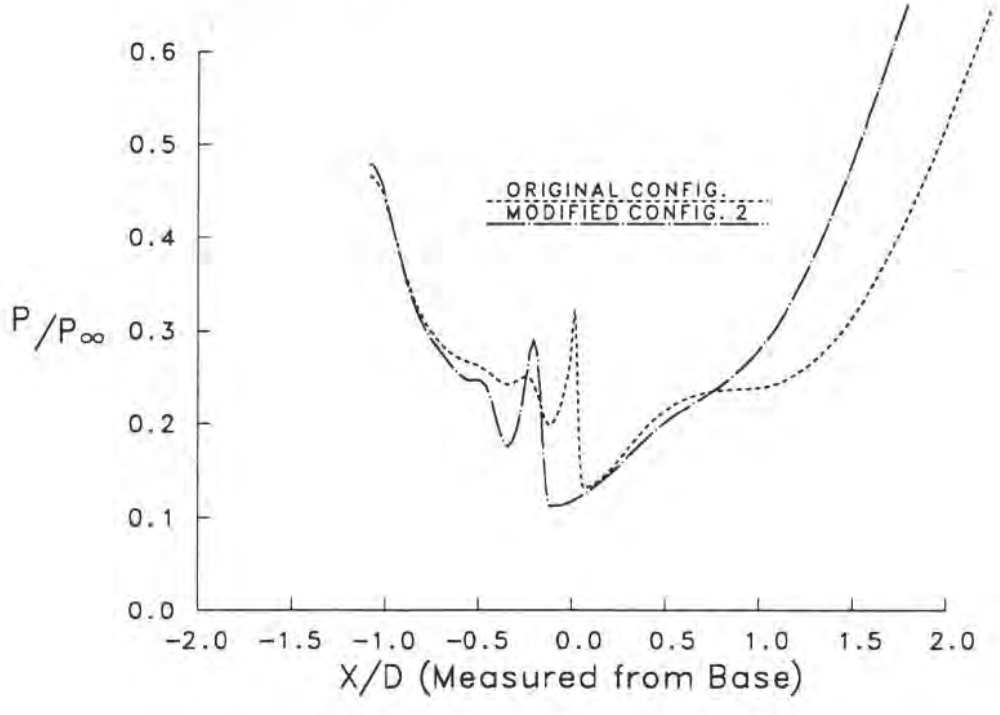

Figure 10. Wake Centerline Pressure distributions, M_∞=3.0, $\alpha = 0.0^0$, (Modified configuration 2).

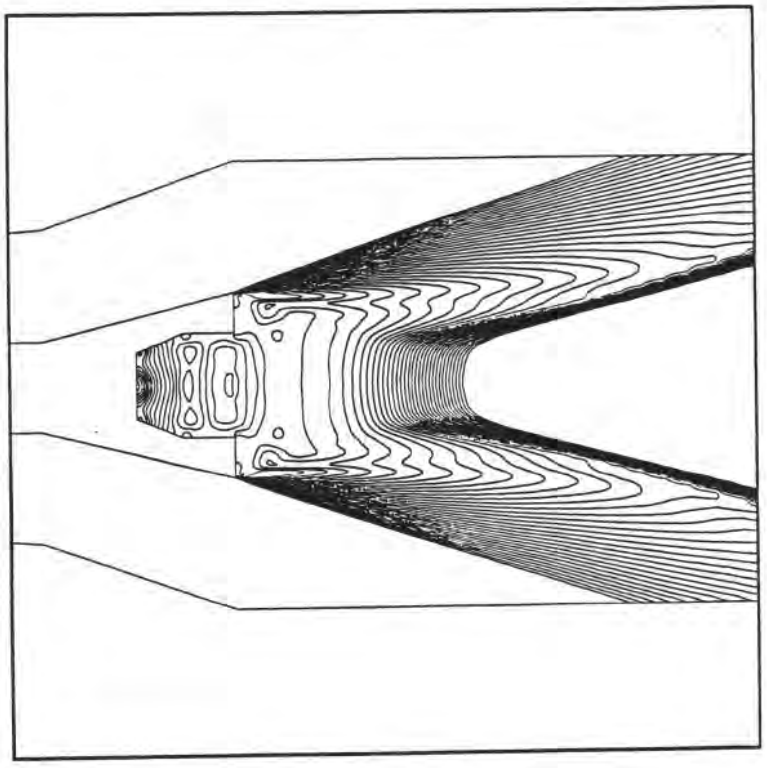

Figure 11. Pressure contours in the base region, M_∞=3.0, $\alpha = 0.0^0$, (Modified configuration 3).

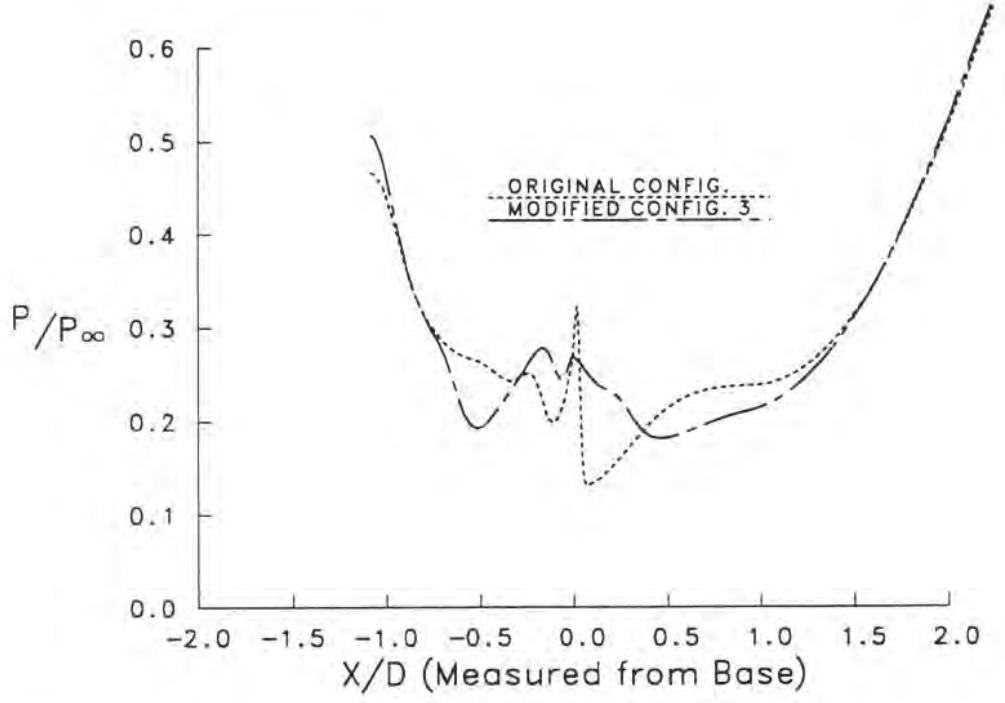

Figure 12. Wake Centerline Pressure distributions, M_∞=3.0, $\alpha = 0.0^0$, (Modified configuration 3).

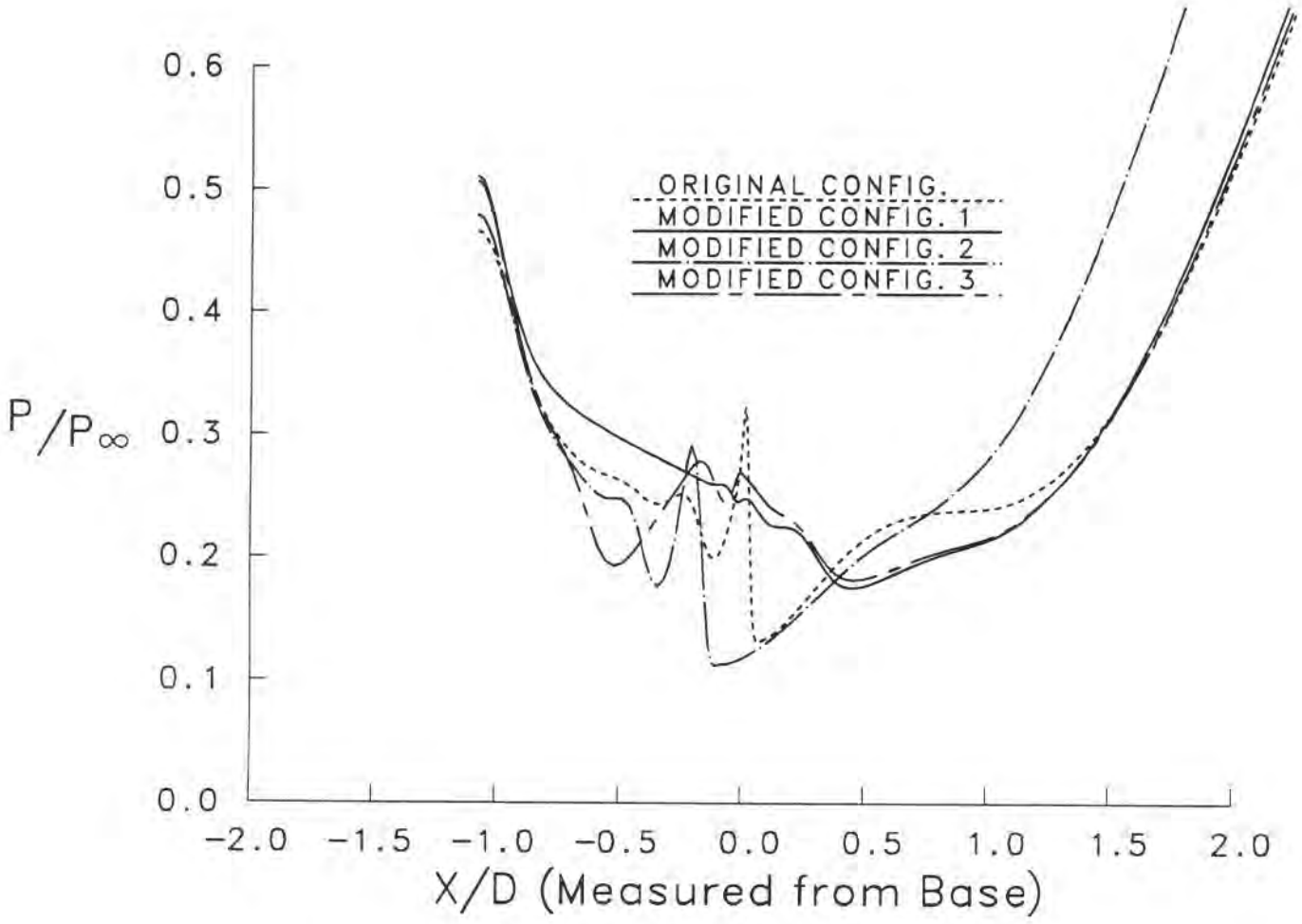

Figure 13. Wake Centerline Pressure distributions, M_∞=3.0, $\alpha = 0.0^0$, (All configurations).

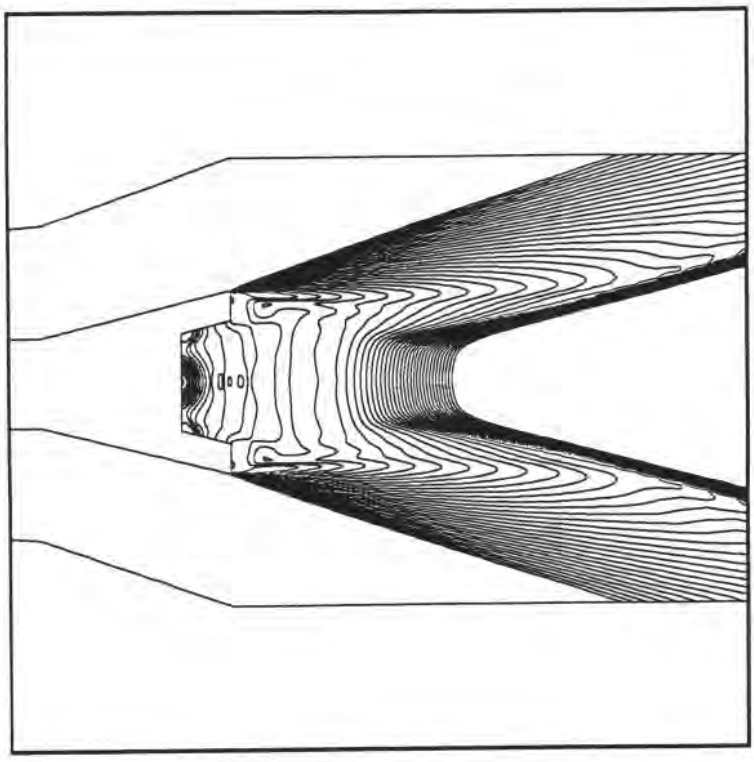

Figure 14. Pressure contours in the base region, M_∞=3.0, $\alpha = 0.0^0$, (ARDEC modified configuration).

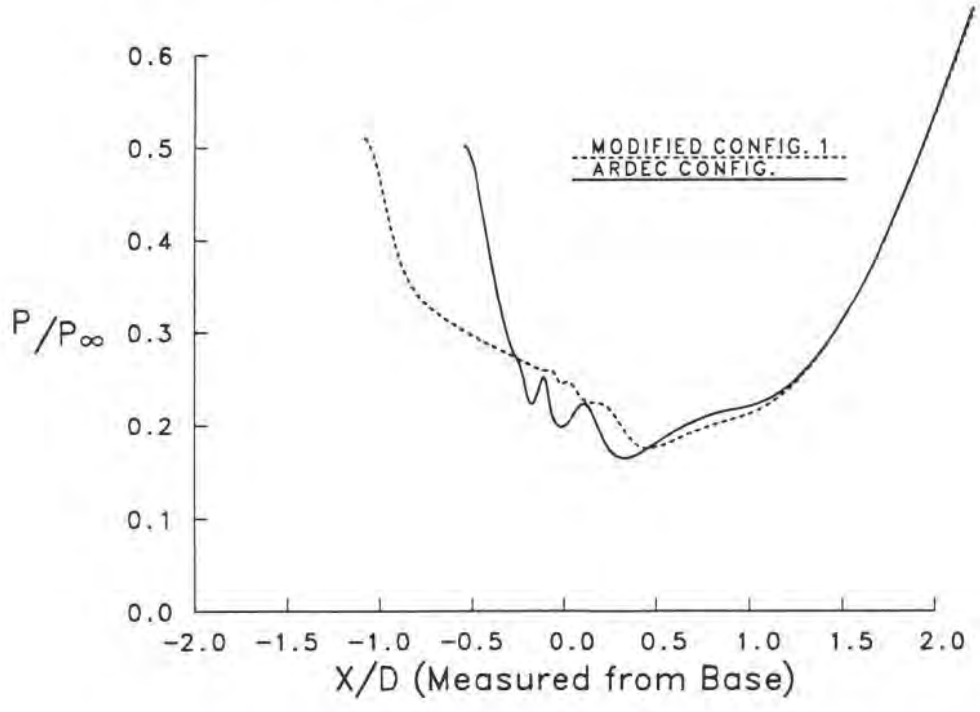

Figure 15. Wake Centerline Pressure distributions, M_∞=3.0, $\alpha = 0.0^0$, (ARDEC modified configuration).

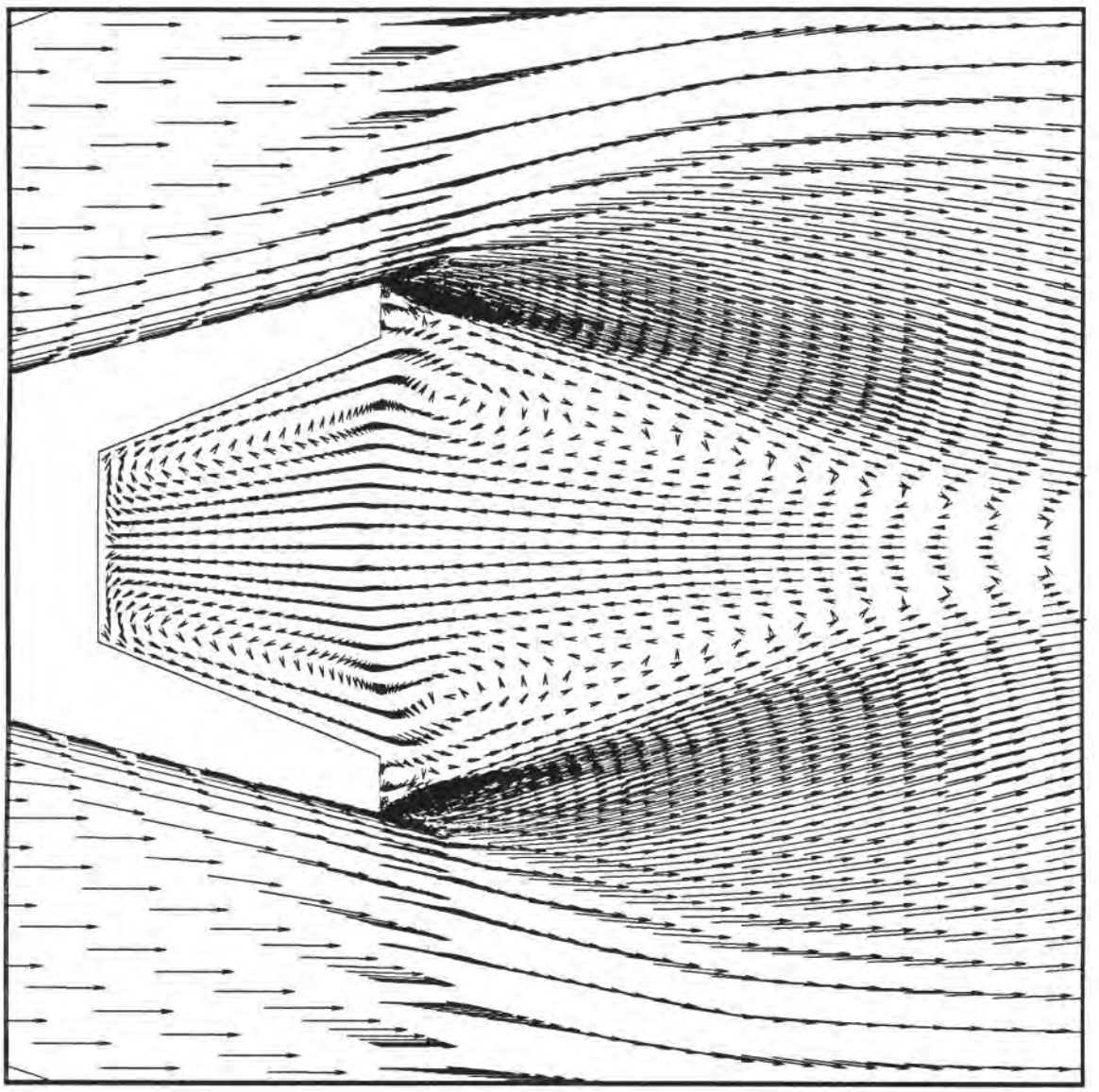

Figure 16. Velocity vectors in the base region, M_∞=3.0, $\alpha = 0.0^0$, (Original configuration).

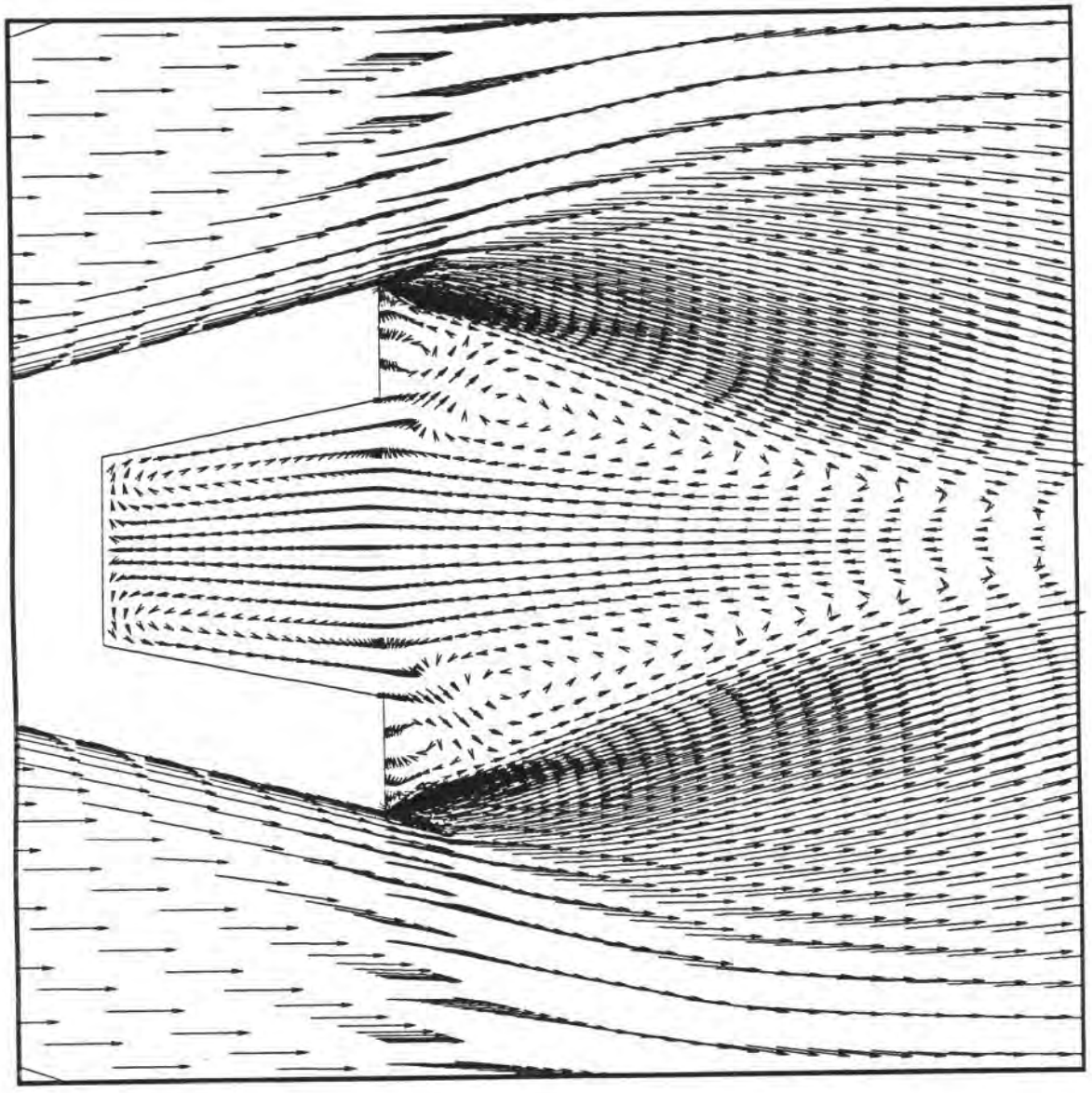

Figure 17. Velocity vectors in the base region, M_∞=3.0, $\alpha = 0.0^0$, (Modified configuration 1).

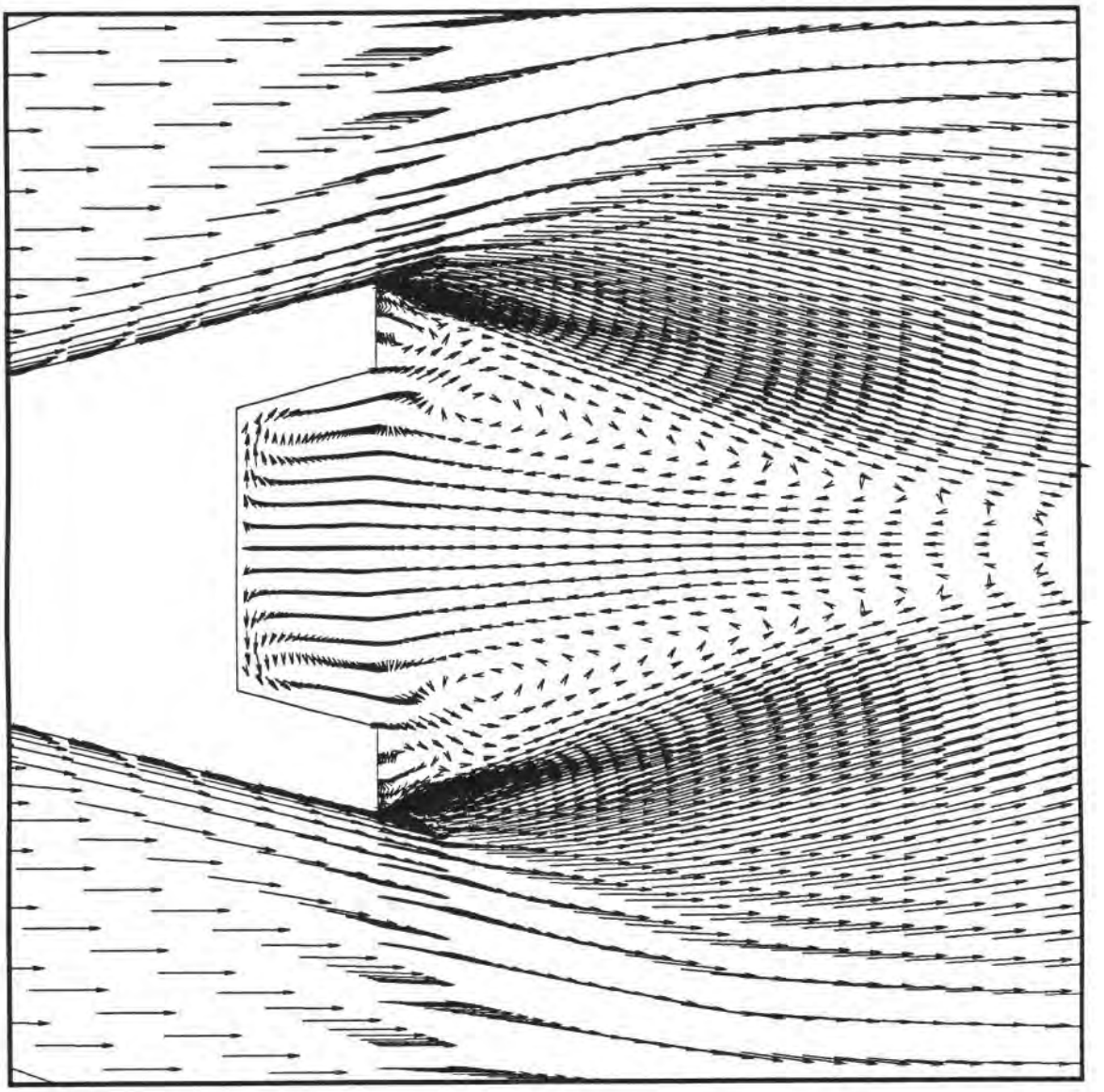

Figure 18. Velocity vectors in the base region, M_∞=3.0, $\alpha = 0.0^0$, (ARDEC configuration).

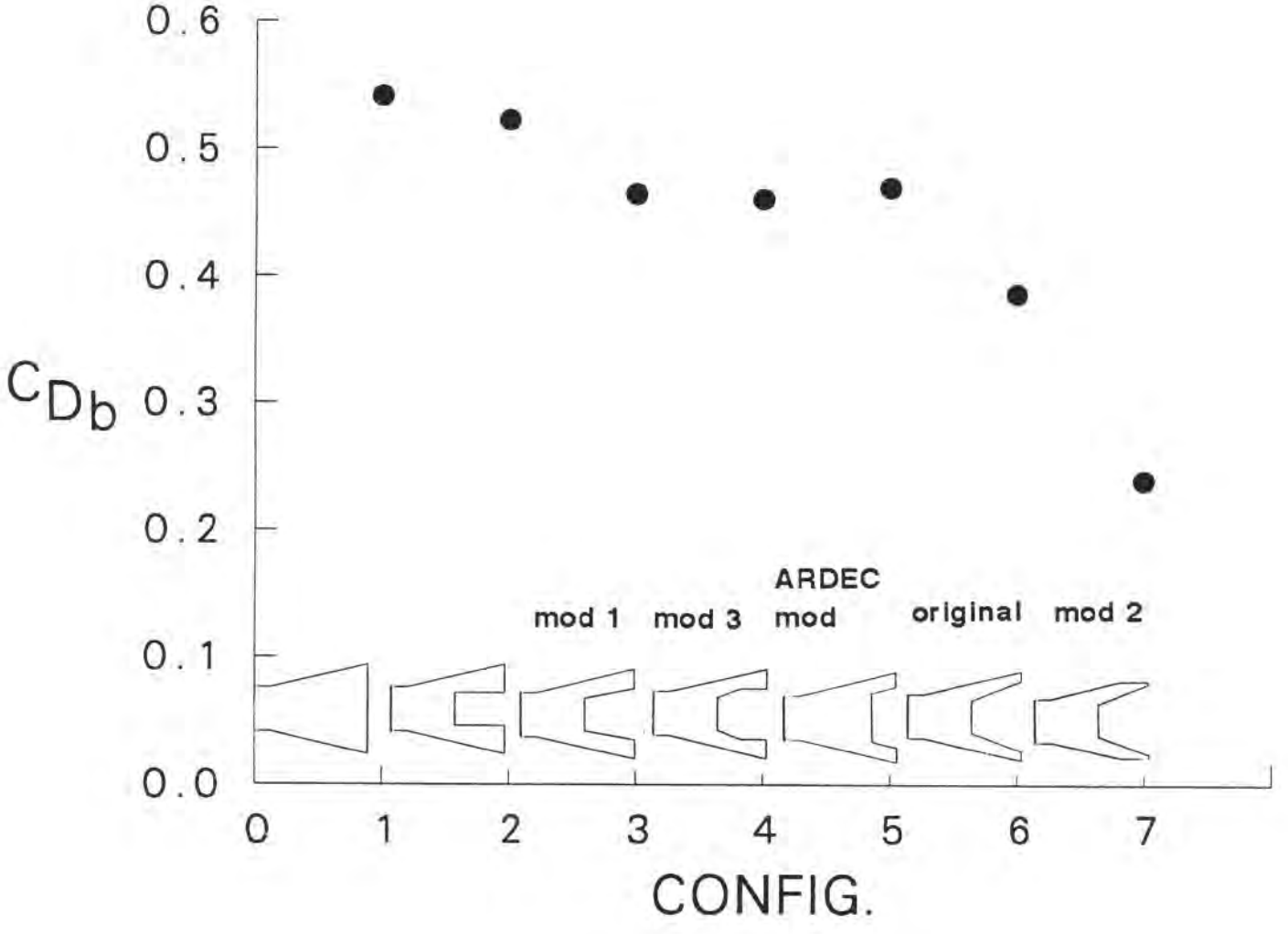

Figure 19. Base drag vs. configuration, M_∞=3.0, $\alpha = 0.0^0$, (All configurations).

Following page intentionally left blank

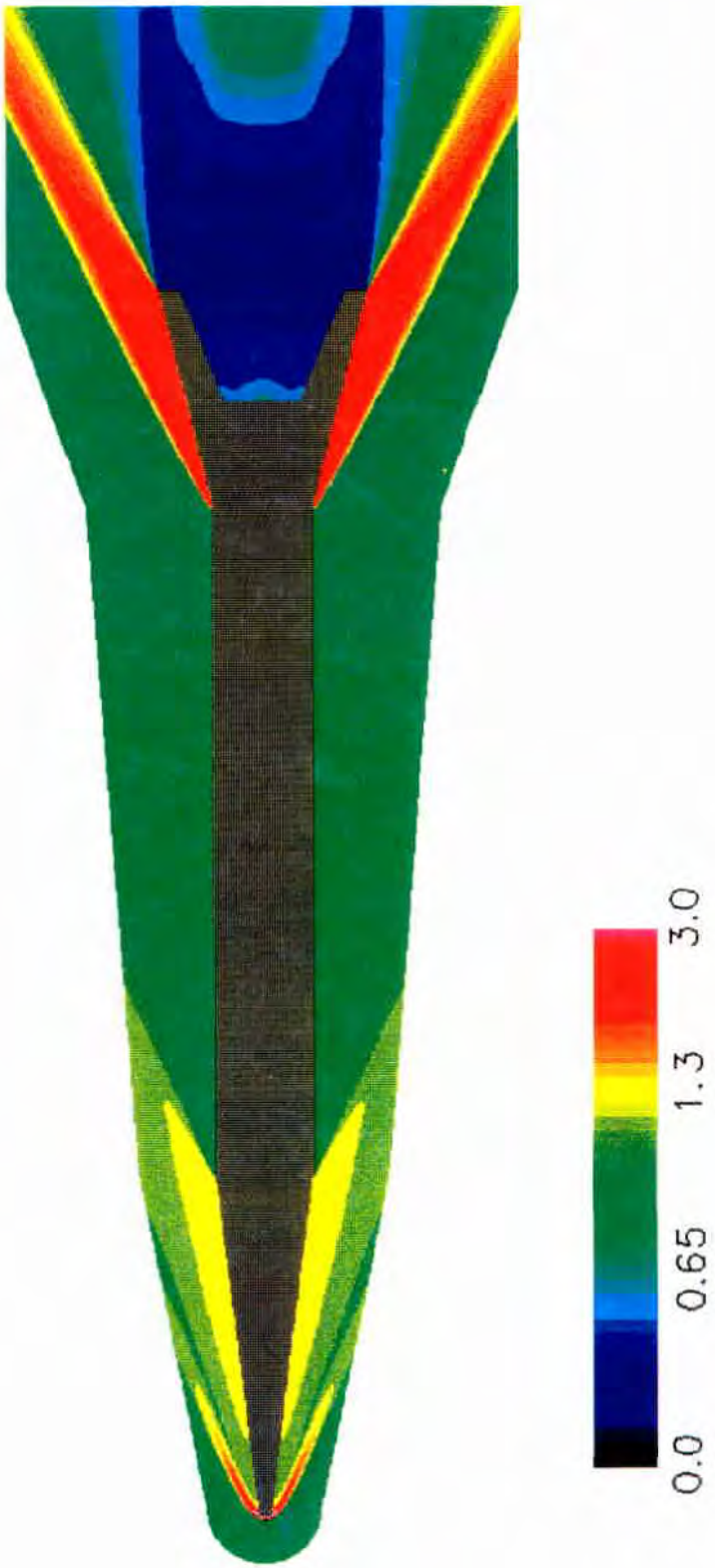

Figure 20. Pressure contours for the entire projectile, M_∞=3.0, $\alpha = 0.0^0$, (original configuration).

Following page intentionally left blank

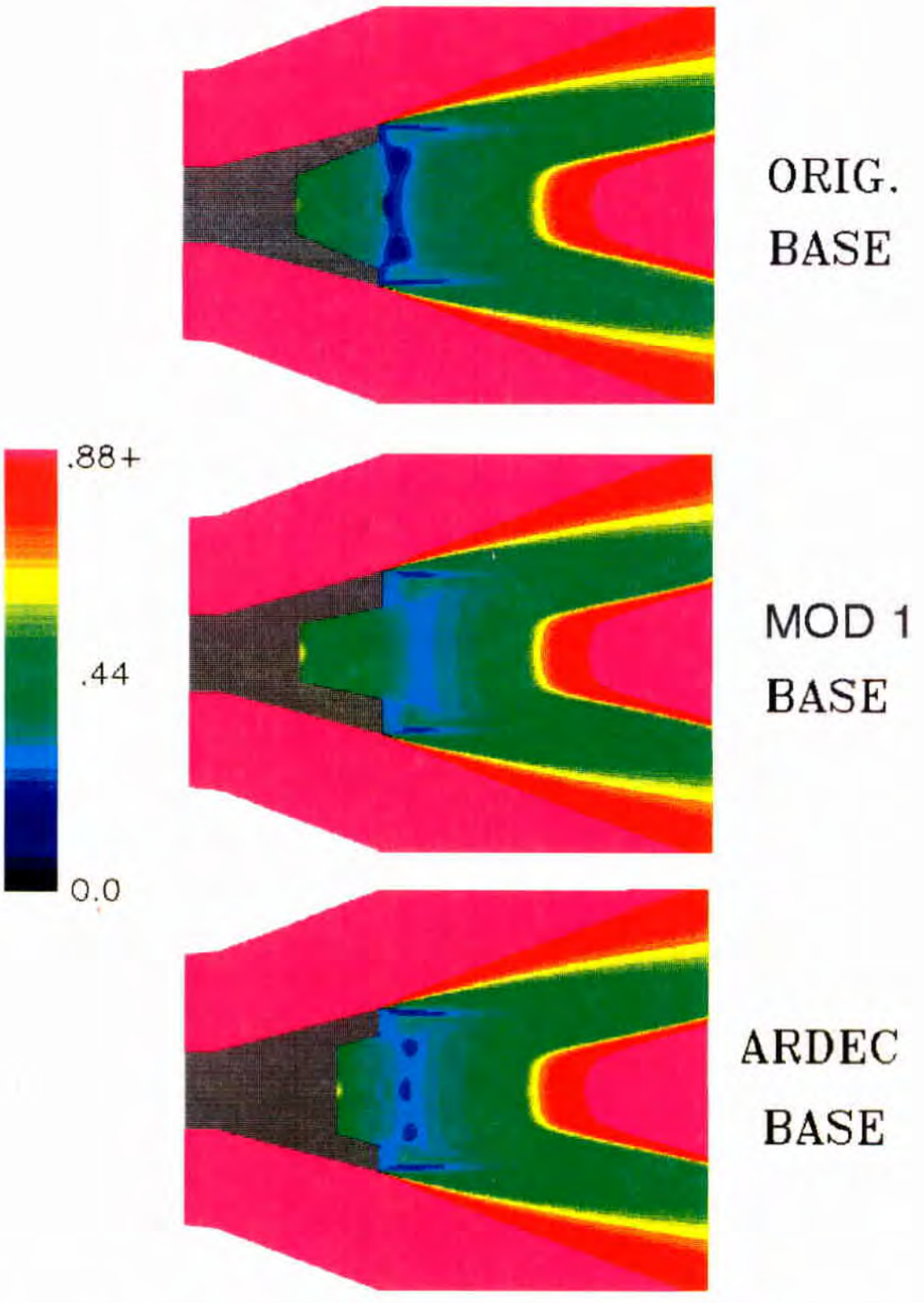

Figure 21. Pressure contours in the base region, M_∞=3.0, $\alpha = 0.0^0$, (original, modified 1, and ARDEC modified configurations).

Following page intentionally left blank

5. REFERENCES

Baldwin B.S. and H. Lomax, "Thin Layer Approximation and Algebraic Model for Separated Turbulent Flows." AIAA Paper No. 78-257, January 1978.

Pulliam, T.H. and J.L. Steger, "On Implicit Finite-Difference Simulations of Three-Dimensional Flow." AIAA Journal, Vol. 18, No. 2, February 1982, pp. 159-167.

Sahu, J., "Computations of Supersonic Flow over a Missile Afterbody Containing an Exhaust Jet." AIAA Journal of Spacecraft and Rockets , Vol. 24, No. 5, September- October 1987, pp. 403-410.

Sahu, J., "Three Dimensional Base Flow Calculation for a Projectile at Transonic Velocity." BRL-MR-3610, U.S. Army Ballistic research Laboratory, Aberdeen Proving Ground, Maryland, September 1987.

Sahu, J., "Numerical Computations of Transonic Critical Aerodynamic Behavior." Paper No. 88-4038-CP, AIAA/ASME/SIAM/APS 1st National Fluid Dynamics Congress, Cincinnati, Ohio, July 1988, (also see BRL-TR-2962, December 1988).

Sahu, J.and C.J. Nietubicz, "Three Dimensional Flow Calculation for a Projectile with Standard and Dome Bases." BRL-IMR-920, U.S. Army Ballistic research Laboratory, Aberdeen Proving Ground, Maryland, August 1989.

Sahu, J., C.J. Nietubicz, and K.R. Heavey, "Computational Study of the M825 Projectile with Standard and Dome Bases." U.S. Army Ballistic Research Laboratory, BRL-MR-3662, Aberdeen Proving Ground, Maryland, March 1988.

Sahu, J., C.J. Nietubicz, and J.L. Steger, "Navier-Stokes Computations of Projectile Base Flow with and without Base Injection." ARBRL-TR-02532, U.S. Army Ballistic Research Laboratory, Aberdeen Proving Ground, Maryland, November 1983. (AD A125738) (also see AIAA Journal, Vol. 23, No. 9, September 1985, pp. 1348-1355).

Sahu, J. and J.L. Steger, "Numerical Simulation of Three Dimensional Transonic Flows." AIAA Paper No. 87-2293, Atmospheric Flight Mechanics Conference, Monterey, California, August 1987, (also see BRL-TR-2903, March 1988).

INTENTIONALLY LEFT BLANK.

No. of Copies	Organization
2	Administrator Defense Technical Info Center ATTN: DTIC-DDA Cameron Station Alexandria, VA 22304-6145
1	Commander U.S. Army Materiel Command ATTN: AMCAM 5001 Eisenhower Ave. Alexandria, VA 22333-0001
1	Director U.S. Army Research Laboratory ATTN: AMSRL-OP-CI-AD, Tech Publishing 2800 Powder Mill Rd. Adelphi, MD 20783-1145
2	Commander U.S. Army Armament Research, Development, and Engineering Center ATTN: SMCAR-IMI-I Picatinny Arsenal, NJ 07806-5000
2	Commander U.S. Army Armament Research, Development, and Engineering Center ATTN: SMCAR-TDC Picatinny Arsenal, NJ 07806-5000
1	Director Benet Weapons Laboratory U.S. Army Armament Research, Development, and Engineering Center ATTN: SMCAR-CCB-TL Watervliet, NY 12189-4050
(Unclass. only) 1	Commander U.S. Army Rock Island Arsenal ATTN: SMCRI-IMC-RT/Technical Library Rock Island, IL 61299-5000
1	Director U.S. Army Aviation Research and Technology Activity ATTN: SAVRT-R (Library) M/S 219-3 Ames Research Center Moffett Field, CA 94035-1000

No. of Copies	Organization
1	Commander U.S. Army Missile Command ATTN: AMSMI-RD-CS-R (DOC) Redstone Arsenal, AL 35898-5010
1	Commander U.S. Army Tank-Automotive Command ATTN: ASQNC-TAC-DIT (Technical Information Center) Warren, MI 48397-5000
1	Director U.S. Army TRADOC Analysis Command ATTN: ATRC-WSR White Sands Missile Range, NM 88002-5502
1	Commandant U.S. Army Field Artillery School ATTN: ATSF-CSI Ft. Sill, OK 73503-5000
(Class. only) 1	Commandant U.S. Army Infantry School ATTN: ATSH-CD (Security Mgr.) Fort Benning, GA 31905-5660
(Unclass. only) 1	Commandant U.S. Army Infantry School ATTN: ATSH-CD-CSO-OR Fort Benning, GA 31905-5660
1	WL/MNOI Eglin AFB, FL 32542-5000
	Aberdeen Proving Ground
2	Dir, USAMSAA ATTN: AMXSY-D AMXSY-MP, H. Cohen
1	Cdr, USATECOM ATTN: AMSTE-TC
1	Dir, ERDEC ATTN: SCBRD-RT
1	Cdr, CBDA ATTN: AMSCB-CI
1	Dir, USARL ATTN: AMSRL-SL-I
10	Dir, USARL ATTN: AMSRL-OP-CI-B (Tech Lib)

No. of Copies	Organization
5	Commander U.S. Army Armament Research, Development, and Engineering Center ATTN: SMCAR-AET-A, R. Kline R. Botticelli H. Hudgins J. Grau S. Kahn Picatinny Arsenal, NJ 07806-5001
1	Department of the Army Office of the Product Manager 155mm Howitzer, M109A6, Paladin ATTN: SFAE-AR-HI-IP, Mr. R. De Kleine Picatinny Arsenal, NJ 07806-5000
1	Commander U.S. Army Armament Research, Development, and Engineering Center ATTN: SMCAR-CCH-V, Paul Valenti Picatinny Arsenal, NJ 07806-5001
1	Commander Naval Surface Warfare Center Dahlgren Division ATTN: Dr. F. Moore Dahlgren, VA 22448-5000
3	WL/MNME Engerteic Materials Branch ATTN: Stephen C. Korn Bruce Simpson Dave Belk 2306 Perimeter Road, Ste 9 Eglin AFB, FL 32542-5910
3	Commander Naval Surface Warfare Center ATTN: Code R44, Dr. F. Priolo Dr. A. Wardlaw K24, B402-12, Dr. W. Yanta White Oak Laboratory Silver Spring, MD 20903-5000

No. of Copies	Organization
4	Director National Aeronautics and Space Administration Langley Research Center ATTN: Tech Library Mr. D. M. Bushnell Dr. M. J. Hemsch Dr. J. South Langley Station Hampton, VA 23665
6	Director National Aeronautics and Space Administration Ames Research Center ATTN: MS-227-8, L. Schiff MS-258-1, T. Holst D. Chaussee M. Rai P. Kutler P. Buning Moffett Field, CA 94035
1	Director Los Alamos National Laboratory ATTN: Mr. Bill Hogan MS G770 Los Alamos, NM 87545
3	Director Sandia National Laboratories ATTN: Div. 1554, Dr. W. Oberkampf Dr. F. Blottner Div. 1636, Dr. W. Wolfe Albuquerque, NM 87185
2	DARPA ATTN: Dr. Peter Kemmey Dr. James Richardson 3701 North Fairfax Drive Arlington, VA 22203-1714
2	Interferometrics, Inc. 8150 Leesburg Pike ATTN: Rene Larriva Eric L. Strobel Vienna, VA 22180

No. of Copies	Organization
3	Science and Technology Inc. ATTN: Dr. Alan Glasser Mr. Bruce Lohman Mr. Dave Maurizi Arlington, VA 22203-1618
1	IAT ATTN: Curt Ober 4030-2 West Braker Lane Austin, TX 78759-5329
3	University of California, Davis Department of Mechanical Engineering ATTN: Prof. H. A. Dwyer Prof. M. Hafez Dr. B. Meakin Davis, CA 95616
1	Massachusetts Institute of Technology ATTN: Tech Library 77 Massachusetts Avenue Cambridge, MA 02139
1	Grumann Aerospace Corporation Aerophysics Research Department ATTN: Dr. R. E. Melnik Bethpage, NY 11714
1	AEDC Calspan Field Service ATTN: MS 600, Dr. John Benek Tullahoma, TN 37389
1	VRA, Inc. ATTN: Dr. Clark H. Lewis, President P.O. Box 50 Blacksburg, VA 24613
1	Advanced Technology Center Arvin/Calspan Aerodynamics Research Department ATTN: Dr. M. S. Holden P.O. Box 400 Buffalo, NY 14225
1	Pennsylvania State University Department of Aerospace Engineering ATTN: Dr. G. S. Dulikravich University Park, PA 16802

No. of Copies	Organization
1	University of Illinois at Urbana Champaign Department of Mechanical and Industrial Engineering ATTN: Dr. J. C. Dutton Urbana, IL 61801
1	University of Maryland Department of Aerospace Engineering ATTN: Dr. J. D. Anderson, Jr. College Park, MD 20742
1	University of Notre Dame Department of Aeronautical and Mechanical Engineering ATTN: Prof. T. J. Mueller Notre Dame, IN 46556
1	University of Texas Department of Aerospace Engineering Mechanics ATTN: Dr. D. S. Dolling Austin, TX 78712-1005
1	University of Delaware Department of Mechanical Engineering ATTN: Dr. John Meakin, Chairman Newark, DE 19716
1	University of Florida Department of Engineering Sciences College of Engineering ATTN: Prof. C. C. Hsu Gainesville, FL 32611
	Aberdeen Proving Ground
4	Cdr, ERDEC ATTN: SCBRD-RT, M. Miller J. Molnar D. Wise D. Weber